Correlations between charge radii differences of mirror nuclei and stellar observables

X. Viñas[a,b] et al.

[a]Universitat de Barcelona, Barcelona, Spain
[b]Institut Menorquí d'Estudis, Maó, Spain

QNP, Barcelona, July 9th, 2024

P. Bano et al et al., Phys. Rev. C108, 015802 (2023)
T.R. Routray et al., Phys. Rev. C104, L011302 (2021) and references therein

The Simple Efffective Interaction (SEI)

The finite range simple effective interaction was initially proposed by Behera and collaborators and has the following explicit form for a Yukawa finite range form factor (SEI-Y),

$$\begin{aligned} V_{eff} &= t_0(1+x_0P_\sigma)\delta(\vec{r}) + \frac{t_3}{6}(1+x_3P_\sigma)\left(\frac{\rho(\vec{R})}{1+b\rho(\vec{R})}\right)^{\gamma}\delta(\vec{r}) \\ &+ (W+BP_\sigma - HP_\tau - MP_\sigma P_\tau)\frac{e^{-r/\alpha}}{r/\alpha} + \text{Spin-orbit part} \end{aligned}$$

where a zero-range spin-orbit (SO) interaction depending on a strength parameter W_0 is taken to deal with finite nuclei. The SEI in Eq.(**??**) has 12 parameters in total, namely, $\alpha, \gamma, b, x_0, x_3, t_0, t_3, W, B, H,$ and M plus the spin-orbit strength parameter W_0, which enters in the description of finite nuclei.

Nine of these twelve parameters are fitted to reproduce empirical constraints and microscopical results in nuclear nd neutron matter.

SEI in asymmetric nuclear matter

$$H_T(\rho_n,\rho_p) = \frac{\hbar^2}{2m}\int \left[f_T^n(\mathbf{k}) + f_T^p(\mathbf{k})\right] k^2 d^3k$$

$$+\frac{1}{2}\left[\frac{\varepsilon_0^l}{\rho_0} + \frac{\varepsilon_\gamma^l}{\rho_0^{\gamma+1}}\left(\frac{\rho}{1+b\rho}\right)^\gamma\right]\left(\rho_n^2+\rho_p^2\right) + \left[\frac{\varepsilon_0^{ul}}{\rho_0} + \frac{\varepsilon_\gamma^{ul}}{\rho_0^{\gamma+1}}\left(\frac{\rho}{1+b\rho}\right)^\gamma\right]\rho_n\rho_p$$

$$+\frac{\varepsilon_{ex}^l}{2\rho_0}\int\int \left[f_T^n(\mathbf{k})f_T^n(\mathbf{k}') + f_T^p(\mathbf{k})f_T^p(\mathbf{k}')\right] g\left(|\mathbf{k}-\mathbf{k}'|\right) d^3k d^3k'$$

$$+\frac{\varepsilon_{ex}^{ul}}{2\rho_0}\int\int \left[f_T^n(\mathbf{k})f_T^p(\mathbf{k}') + f_T^p(\mathbf{k})f_T^n(\mathbf{k}')\right] g\left(|\mathbf{k}-\mathbf{k}'|\right) d^3k d^3k',$$

$$g_Y(|\mathbf{k}-\mathbf{k}'|) = (\mathbf{1} + ((\mathbf{k}-\mathbf{k}')/\mathbf{\Lambda})^2)^{-1} \quad \mathbf{g_G}(|(\mathbf{k}-\mathbf{k}')|) = \mathbf{e}^{-\left(\frac{(\mathbf{k}-\mathbf{k}')}{\mathbf{\Lambda}}\right)^2},$$

$$f_T^{n(p)}(\vec{k}) = 1 + exp\left[\left\{\epsilon_T^{n(p)}(k,\rho_n,\rho_p) - \mu_T^{n(p)}\right\}/T\right]^{-1}$$

$$\epsilon_T^{n(p)}(\mathbf{k},\rho_n,\rho_p) = \frac{\hbar^2k^2}{2m} + u_T^{n(p)}(\mathbf{k},\rho_n,\rho_p)$$

$$
\begin{aligned}
H(\rho_n,\rho_p) &= \frac{3\hbar^2}{10m}\left(k_n^2\rho_n + k_p^2\rho_p\right) + \frac{\varepsilon_0^l}{2\rho_0}\left(\rho_n^2+\rho_p^2\right) + \frac{\varepsilon_0^{ul}}{\rho_0}\rho_n\rho_p \\
&+ \left[\frac{\varepsilon_\gamma^l}{2\rho_0^{\gamma+1}}\left(\rho_n^2+\rho_p^2\right) + \frac{\varepsilon_\gamma^{ul}}{\rho_0^{\gamma+1}}\rho_n\rho_p\right]\left(\frac{\rho(\mathbf{R})}{1+b\rho(\mathbf{R})}\right)^\gamma \\
&+ \frac{\varepsilon_{ex}^l}{2\rho_0}\rho_n^2\left[\frac{3\Lambda^6}{16k_n^6} - \frac{9\Lambda^4}{8k_n^4} + \left(\frac{3\Lambda^4}{8k_n^4} - \frac{3\Lambda^6}{16k_n^6}\right)e^{-4k_n^2/\Lambda^2}\right] \\
&+ \frac{\varepsilon_{ex}^l}{2\rho_0}\rho_p^2\left[\frac{3\Lambda^6}{16k_p^6} - \frac{9\Lambda^4}{8k_p^4} + \left(\frac{3\Lambda^4}{8k_p^4} - \frac{3\Lambda^6}{16k_p^6}\right)e^{-4k_p^2/\Lambda^2}\right] \\
&+ \frac{3\sqrt{\pi}\varepsilon_{ex}^l}{4\rho_0}\left[\frac{\Lambda^3}{k_n^3}\rho_n^2 erf\left(\frac{2k_n}{\Lambda}\right) + \frac{\Lambda^3}{k_p^3}\rho_p^2 erf\left(\frac{2k_p}{\Lambda}\right)\right] \\
&+ \frac{3\varepsilon_{ex}^{ul}}{8\rho_0}\rho_n\rho_p\frac{\Lambda}{k_n}\frac{\Lambda}{k_p}\Bigg\{\left[\frac{\Lambda^2}{k_n^2} + \frac{\Lambda^2}{k_p^2} - \frac{\Lambda}{k_n}\frac{\Lambda}{k_p} - \frac{1}{2}\right]\left(e^{-\left(\frac{k_n+k_p}{\Lambda}\right)^2} - e^{-\left(\frac{k_n-k_p}{\Lambda}\right)^2}\right) \\
&\sqrt{\pi}\left[\frac{\Lambda^2}{k_n^2} + \frac{\Lambda^2}{k_p^2} - \frac{\Lambda}{k_n}\frac{\Lambda}{k_p}\right]\left(\frac{k_n+k_p}{\Lambda}erf\left(\frac{k_n+k_p}{\Lambda}\right) - \frac{k_n-k_p}{\Lambda}erf\left(\frac{k_n-k_p}{\Lambda}\right)\right)\Bigg\}
\end{aligned}
$$

Fitting protocol

- The symmetric nuclear matter (SNM) requires only the following three combinations of the strength parameters,

$$\left(\frac{\varepsilon_0^l + \varepsilon_0^{ul}}{2}\right) = \varepsilon_0, \left(\frac{\varepsilon_\gamma^l + \varepsilon_\gamma^{ul}}{2}\right) = \varepsilon_\gamma, \left(\frac{\varepsilon_{ex}^l + \varepsilon_{ex}^{ul}}{2}\right) = \varepsilon_{ex},$$

  which together with γ, b and α constitute the six parameters for the SNM. For a given value of the exponent γ, which characterizes as the stiffness parameter and determines the incompressibil
- It is demanded that he nuclear mean-field in symmetric nuclear matter at saturation vanished for a kinetic energy of incident nucleaon of 300 MeV. This constraint allows to determine, for a given value of γ, the strength of the excahnege energy, ε_{ex}, and the range of the form factor α.
- The parameter b is determined to avoid the supra-luminous behaviour.
- The two remaining parameters, ε_0 and ε_γ are obtained from given saturation conditions. (density nd energy per baryon)

- The splitting of the exchange strength is decided to be $\varepsilon_{ex}^{l} = 2\varepsilon_{ex}^{ul}/3$, which ensures that the entropy in pure neutron matter does not exceed that of symmetric nuclear matter.
- The splitting of the parameters ε_0 and ε_γ is decided from the value oif the symmetry energy and its slope.
- The characteristic slope of the symmetry energy is fixed from the condition that the asymmetric contribution to the nucleonic part of the energy density in charge neutral beta-stable stellaar matter $npe\mu$ is maximal.
- One of the two free parameters, x_0, is fixed from the spin-up and spin-down splitting of the effective mass in polatized neutron matter.
- Finally the parameter t_0 and the spin-orbit strength W_0 are determined from calculations in finite nuclei.

Neutron-rich Ni isotopoes

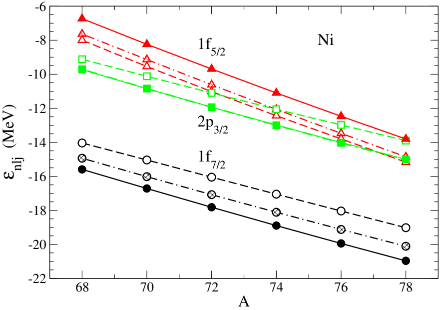

Proton single-particle levels around the Fermi level for Ni isotopes from A=68 to A=78 computed with the Skyrme forces SAMi-T and SLy5 with two different tensor contributions.

SAMi-T : S. Shen et al, Phys.Rev.**C99**,034322 (2019) (dashed)

SLy5 : G.Colò et al, Phys.Lett.B646,227 (2007) (solid), M. Grasso and M. Anguiano, Phys.Rev.**C88**,054328 (2013) (dash-dotted)

Neutron-rich Ni isotopoes

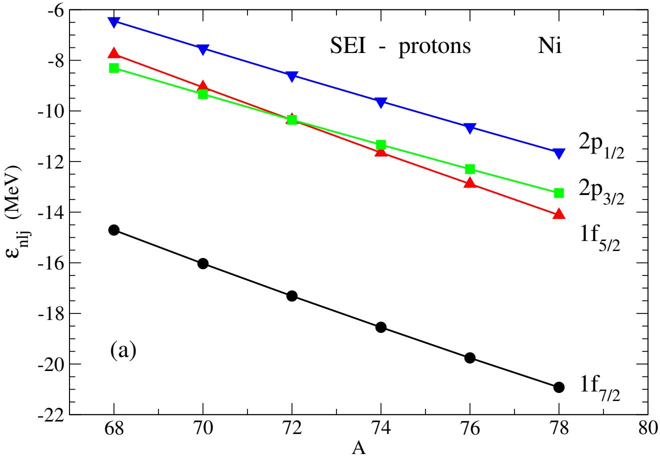

Proton single-particle levels around the Fermi level for Ni isotopes from A=68 to A=78 computed with SEI.

SEI B.Behera et al, J.of Phys.G **40**,095105 (2013)

Table: Ground-state spin and energy of neutron-rich odd Cu isotopes predicted by the SEI model used in this work. The energy of the first excited state E^* is shown for the SEI model. The experimental energies (K.T. Flanagan et al, Phys.Rev.Lett.**103**, 14250 (2009) are also reported for comparison. Notice that according to the experimental data, the spin-parity of the ground-state of the nucleus ^{75}Cu is $5/2^-$ and the first excited state $3/2^-$ 62 keV above.

Nucleus	Spin-Parity	Energy(SEI) (MeV)	Energy(exp) (MeV)	E^*(SEI) (keV)	E^*(exp) (keV)
^{69}Cu	$3/2^-$	−598.59	−599.97	794	1215
^{71}Cu	$3/2^-$	−612.93	−613.09	544	537
^{73}Cu	$3/2^-$	−625.76	−625.51	282	263
^{75}Cu	$3/2^-$	−637.49	−637.13	72	62
^{77}Cu	$3/2^-$	−648.38	−647.42	246	295
^{79}Cu	$5/2^-$	−658.19	−656.65	525	660

Charge radii and neutron skin in mirror nuclei (I)

- Under strict isospin symmetry the neutron skin thickness in a nucleus becomes the proton mass difference between in a mirror nuclei pair $\Delta R_p = R_p(N,Z) - R_p(Z,N)$
- When Coulomb and other symmetry breaking effects ar takwn into account, the neutron skin thickness and the difference of proton radii in the mirror pair are correlated as:

$$\Delta R_{np} = (0.881 \pm 0.036)\Delta R_p + (-0.049 \pm 0.017)\text{fm}$$

ΔR_{CH}(Expt)[fm]	^{34}Ar-^{34}S	^{36}Ca-^{36}S	^{38}Ca-^{38}Ar	^{54}Ni-^{54}Fe
	0.082(9)	0.150(4)	0.063(3)	0.049(4)
ΔR_{CH}(SEI)[fm]	^{34}Ar-^{34}S	^{36}Ca-^{36}S	^{38}Ca-^{38}Ar	^{54}Ni-^{54}Fe
	0.087	0.147	0.066	0.049

Table: Experimental results for the charge radii difference of mirror pair nuclei and the predictions of the characteristic SEI EoS having $L = 76.71$ MeV.

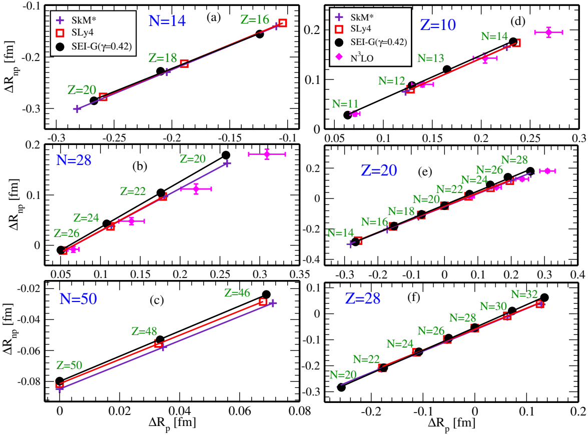

Linear correlation between the neutron skin ΔR_{np} and the proton *rms* radii difference ΔR_p for mirror nuclei pairs shown for the SEI EoS in the isotonic chains of (a) N=14, (b) N=28, and (c) N=50 and isotopic chains ¿ (d) Z=10, (e) Z=28 and (f) Z=50. The results of SkM*, SLy4 and N^{3}LO forces are given by symbols plus (indigo), square (red) and diamond (magenta), respectively

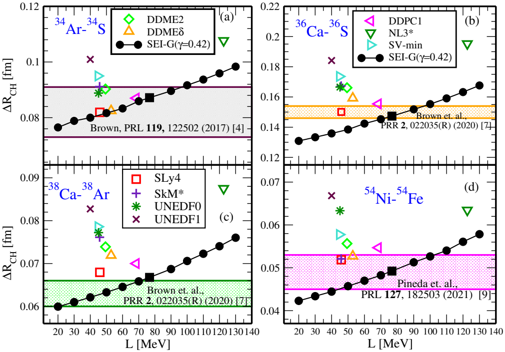

ΔR_{CH} as a function of the symmetry energy slope L for the mirror pairs (a)^{34}Ar-^{34}S, (b)^{36}Ca-^{36}S, (c)^{38}Ca-^{38}Ar, and (d)^{54}Ni-^{54}Fe. The experimental results are shown in horizontal bands in each panel. The SEI characteristic EoS results are shown by filled squares in the four panels, whereas the results for SEI EoSs other than L=L$_C$ are in black filled circles.

	ΔR_{CH}(fm)			
	^{34}Ar-^{34}S	^{36}Ca-^{36}S	^{38}Ca-^{38}Ar	^{54}Ni-^{54}Fe
Expt:	0.082(9) [?]	0.150(4) [?]	0.063(3) [?]	0.049(4) [?]
SEI:	0.087	0.147	0.066	0.049

Table: Experimental results for the charge radii difference of mirror pair nuclei and the predictions of the characteristic SEI EoS having $L = 76.71$ MeV.

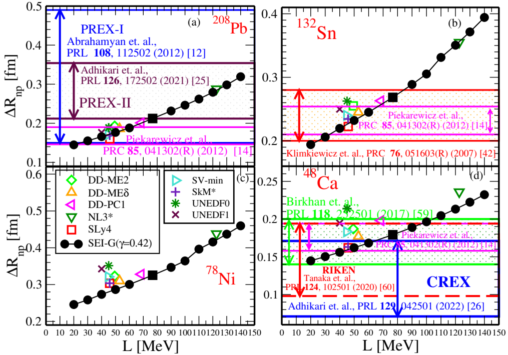

Neutron skin thickness ΔR_{np} as a function of L for (a) ^{208}Pb, (b) ^{132}Sn, (c) ^{78}Ni, and (d) ^{48}Ca for SEI-G($\gamma = 0.42$). The results extracted from theoretical analyses of the experiments are shown in horizontal bands in each panel where available.

Nuclear charge radii and neutron star observables

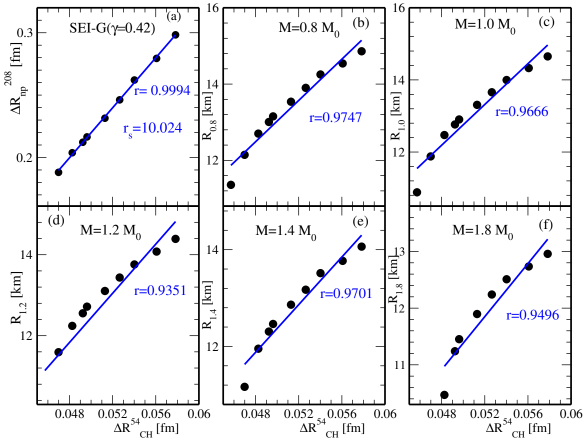

Stellar radii for neutron stars having masses (b) M=0.8 $M_\odot$, (c) 1.0 $M_\odot$, (d) 1.2 $M_\odot$, (e) 1.4 $M_\odot$, and (f) 1.8 $M_\odot$ as a function of the charge radii difference ΔR_{CH}^{54} between the ^{54}Ni and ^{54}Fe pair. The correlation between ΔR_{CH}^{54} and ΔR_{np}^{208} (skin thickness of ^{208}Pb) is shown in panel (a).

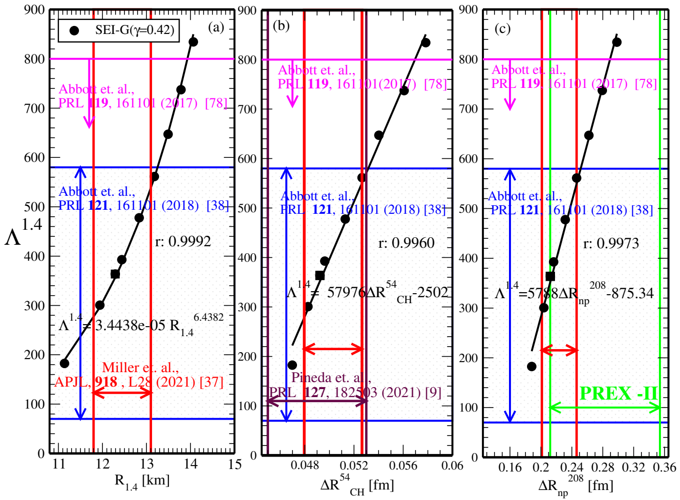

Tidal deformability, $\Lambda^{1.4}$, in $1.4M_\odot$ NSs versus (a) the radius $R_{1.4}$ of $1.4M_\odot$ NSs, (b) charge radii difference ΔR^{54}_{CH} of the ^{54}Ni-^{54}Fe mirror pair, and (c) neutron skin thickness ΔR^{208}_{np} in ^{208}Pb.